ELSEVIER

Biophysical Chemistry 78 (1999) 21–32

Biophysical Chemistry

Temperature dependence of the solubility of non-polar gases in water

Shekhar Garde*, Angel E. García, Lawrence R. Pratt, Gerhard Hummer

Theoretical Division, Los Alamos National Laboratory, Los Alamos, New Mexico 87545, USA

Received 21 August 1998; received in revised form 18 January 1999; accepted 18 January 1999

Abstract

An explanation is provided for the experimentally observed temperature dependence of the solubility and the solubility minimum of non-polar gases in water. The influence of solute size and solute–water attractive interactions on the solubility minimum temperature is investigated. The transfer of a non-polar solute from the ideal gas into water is divided into two steps: formation of a cavity in water with the size and shape of the solute and insertion of the solute in this cavity which is equivalent to 'turning on' solute–water attractive interactions. This two step process divides the excess chemical potential of the non-polar solute in water into repulsive and attractive contributions, respectively. The reversible work for cavity formation is modeled using an information theory model of hydrophobic hydration. Attractive contributions are calculated by modeling the water structure in the vicinity of non-polar solutes. These models make a direct connection between microscopic quantities and macroscopic observables. Moreover, they provide an understanding of the peculiar temperature dependences of the hydration thermodynamics from properties of pure water; specifically, bulk water density and the water oxygen–oxygen radial distribution function.

1. Introduction

Hydrophobic hydration and the interaction of hydrophobic solutes in aqueous media have attracted considerable attention as a result of their role in stabilizing folded proteins as well as micelles, membranes, and macromolecular assemblies [1–4]. Phase behavior of proteins and assemblies of amphiphilic molecules show peculiar variations with temperature and pressure. Heat, pressure, or cold denaturation of proteins [5–8], as well as variation of critical micelle concentration (CMC) with temperature and the length of the hydrophobic tail of surfactants [9] are examples where hydrophobic effects play an important role in macromolecular stability. A quantitative description of the temperature and pressure dependence of hydrophobic phenomena for simple non-polar solutes has given insights into the thermodynamic stability of more complicated systems,

* Corresponding author. Tel: +1-505-655-3853; fax: +1-505-665-3493, e-mail: garde@lanl.gov

0301-4622/99/$ - see front matter
PII: S0301-4622(99)00018-6

such as proteins and micelles. One example is the convergence of entropies of unfolding of globular proteins with increasing temperature that has also been observed for the transfer of simple hydrophobic solutes from gas phase into water [6]. Application of an information theory model to hydrophobic hydration not only offered a quantitative explanation of the entropy convergence for simple hydrophobic solutes but also provided insights into the origin of entropy convergence in protein unfolding [10]. The observations made about the origin of entropy convergence at a microscopic level using a molecular theory also hold when viewed from a macroscopic perspective. Specifically, the equation of state of bulk water provides essential elements of a qualitative explanation.

A well known peculiarity of hydrophobic hydration is the non-monotonic temperature dependence of the solubility of non-polar solutes in water [11]. As temperature is increased from near room temperature, the solubility of many non-polar gases in water decreases before reaching a minimum and then increasing again at higher temperatures. Both macroscopic thermodynamic models and extensive calculations based on computer simulations of hydrophobic solubilities in water have been used previously to describe this behavior [12,13]. Although the solubility minimum of non-polar gases in water has been observed in these simulations [13], a satisfactory molecular explanation of this phenomenon has been elusive [14].

In this paper, we focus specifically on the solubility minimum of non-polar gases in water with increasing temperature. We use perturbation theory ideas analogous to those used in the Pratt–Chandler theory [15,16] in combination with the information theory approach [17]. These theories are used to model contributions to the excess chemical potential arising from repulsive and attractive solute–water interactions. Chemical potentials of spherical Lennard–Jones (LJ) solutes in the size range of noble gases, and their Weeks–Chandler–Andersen [18] (WCA) and hard-sphere (HS) equivalents are calculated by extensive test particle insertions in pure liquid water configurations over a range of temperatures. This separation allows us to formulate a molecular explanation for the existence of solubility minima. We also illustrate how solute–water repulsive interactions (i.e. solute size) and solute–water attractive interactions affect the temperature at which the solubility minimum occurs. Finally, we comment on how the modeling presented here is directly relevant to the observed minimum in the CMC with increasing temperature for ionic as well as non-ionic surfactants. The dependence of the temperature of minimum CMC on the length of hydrophobic and hydrophilic parts of non-ionic surfactants is also explained qualitatively.

2. Theory

The transfer of a hydrophobic solute from an ideal gas phase into water can be divided into two steps: formation of a cavity in water with the size and shape of the solute and insertion of the solute in this cavity which is equivalent to 'turning on' solute–water attractive interactions [11,19]. The process of creating a cavity in a liquid is unfavorable and the corresponding free energy positive. The latter contribution is usually favorable owing to the solute–water attractive interactions. This two step process divides the excess chemical potential of the non-polar solute in water into repulsive and attractive contributions, respectively. Our goal in this paper is to obtain a simple representation of the excess chemical potential of a LJ solute in water as well as its temperature dependence. In obtaining such a representation, exhaustive computer simulation data and molecular theories are used to gain insight. Ultimately we strive for an explanation based on macroscopic observable properties of pure water together with some simple structural information.

2.1. Perturbation theory

The excess chemical potential of a LJ solute can be calculated using the expression [20,21],

$$\exp\left[-\frac{(\mu_{LJ}^{ex}-\mu_0^{ex})}{k_BT}\right]=\left\langle\exp\left(-\frac{u_{att}}{k_BT}\right)\right\rangle_0, \qquad (1)$$

where 0 indicates a reference solute with purely repulsive solute–water interaction energy u_0, $u_{att}(=u_{LJ}-u_0)$ is the difference between *LJ*–water and reference solute–water interaction energies, and $\langle\cdots\rangle_0$ indicates canonical thermal averaging over the reference system Hamiltonian. Also, k_B is Boltzmann's constant, and the superscript '*ex*' indicates an excess chemical potential with respect to the ideal gas phase for both the *LJ* and the reference solute. Expanding Eq. (1) in terms of cumulants [20] of u_{att} we obtain

$$\mu_{LJ}^{ex}=\mu_0^{ex}+\langle u_{att}\rangle_0-\frac{1}{2k_BT}\mathrm{var}(u_{att})+\cdots, \qquad (2)$$

where $\mathrm{var}(u_{att})$ indicates the variance of u_{att} in the reference state 0. The higher order terms are the cumulants of order three and larger for the distribution of u_{att} in the reference state. A reference state that has been successful in describing the properties of condensed liquid systems was introduced by Weeks, Chandler, and Andersen [18]. The short-range solute–water repulsive interactions are defined as:

$$u_{WCA}(r)=\begin{cases}u_{LJ}(r)+\epsilon & \text{for } r<2^{1/6}\sigma\\ 0 & \text{otherwise.}\end{cases} \qquad (3)$$

where σ and ϵ are size and energy parameters for an *LJ* interaction, respectively, and the subscript *WCA* indicates the reference solute. The remaining attractive part of the solute–water interactions is:

$$u_{att}(r)=\begin{cases}-\epsilon & \text{for } r<2^{1/6}\sigma\\ u_{LJ}(r) & \text{otherwise,}\end{cases} \qquad (4)$$

and,

$$u_{LJ}(r)=4\epsilon\left[\left(\frac{\sigma}{r}\right)^{12}-\left(\frac{\sigma}{r}\right)^{6}\right]. \qquad (5)$$

For such a separation, the structural organization of water around an *LJ* solute and that around the corresponding *WCA* solute will be similar, with repulsive interactions dominating the hydration structure [16]. Note that this separation into attractive and repulsive interactions for a condensed system is reasonable but not unique. Only the first order perturbation term is expected to contribute significantly to the excess chemical potential in addition to the reference term in Eq. (2). Therefore, we write

$$\mu_{LJ}^{ex}\approx\mu_{WCA}^{ex}+\langle u_{att}\rangle_{WCA}. \qquad (6)$$

This equation gives an approximate separation of the chemical potential into repulsive and attractive contributions. In the following, we model each of these terms using readily available information for model systems.

The chemical potential of a *WCA* solute can be approximated by the chemical potential of a *HS* solute of equivalent radius. Many possible prescriptions are available for determining the 'equivalent' *HS* radius corresponding to a given continuous potential [22][1]. For example, a thermodynamic definition can be chosen such that the free energies of *HS* and *WCA* systems are approximately equal. Here we choose the equivalent *HS* radius based on the water structure in the vicinity of *WCA* solutes. The smallest distance at which the solute–water radial distribution function reaches the value of one is chosen as the sum of the solute and water *HS* radii, or equivalently, the cavity radius for a given solute [17]. Estimates of equivalent *HS* radii for different solutes are obtained from preliminary test particle insertion calculations. Note that the resulting *HS* radius is weakly temperature dependent. Once the equivalent *HS* radius is chosen, we use the information theory approach to model the repulsive part of the excess chemical potential as described below.

[1]We note that the specific choice of the equivalent hard sphere radius will not affect the general conclusions on the temperature dependence of the solubility of hydrophobic solutes obtained in this paper.

2.2. Information theory approach to HS chemical potentials

The excess chemical potential, μ_{HS}^{ex}, of a hard-core solute in water is related to the probability, p_0, of forming a cavity in water with the size and shape of the solute by [23]

$$\mu_{HS}^{ex} = -kT \ln p_0. \tag{7}$$

For a successful insertion of a spherical hard-core solute with radius r_{HS}, the water oxygens must be excluded from a spherical volume of radius $r = r_{HS} + r_W$, where r_W is the equivalent hard-core radius of a water molecule. For convenience, we will focus on the cavity radius r in the discussion that follows.

Here we outline only the salient features of the information theory approach for calculating p_0, which has been discussed in detail elsewhere [17,24]. Formation of a cavity constitutes a fluctuation in the equilibrium density of the bulk fluid. A given molecular volume v contains, on average, a number ρv of solvent particles, where ρ is the number density of solvent particles in bulk phase. The number of particles in the observation volume fluctuates. The information theory approach models the distribution p_n, the probability of observing exactly n solvent centers inside a given molecular volume v. Information about the moments of this distribution is used as constraints in a maximum entropy formulation to provide the 'best possible' description of p_n that satisfies those constraints. The quantity of interest, p_0, the probability of observing 0 solvent centers in the molecular volume v is then just one of the elementary events.

The kth moment of the particle number distribution given by

$$\langle n^k \rangle = \sum_{n=0}^{\infty} n^k p_n \tag{8}$$

is related to the kth order particle–particle correlation function in the bulk solvent. In particular, the 0th, 1st, and 2nd moment can be expressed in terms of experimentally available quantities:

$$\langle 1 \rangle = \sum_{n=0}^{\infty} p_n = 1 \tag{9}$$

$$\langle n \rangle = \sum_{n=0}^{\infty} n p_n = \rho v \tag{10}$$

$$\langle n^2 \rangle = \sum_{n=0}^{\infty} n^2 p_n = \rho v + \rho^2 \int_v d\mathbf{r} \int_v d\mathbf{r}' g(|\mathbf{r} - \mathbf{r}'|), \tag{11}$$

where $\langle \cdots \rangle$ denotes the canonical average and $g(|\mathbf{r} - \mathbf{r}'|)$ is the water oxygen–oxygen radial distribution function in the bulk water phase.

To obtain the best possible description of p_n, the relative or cross entropy η given by [25]

$$\eta(\{p_n\}) = -\sum_{n=0}^{\infty} p_n \ln\left(\frac{p_n}{\hat{p}_n}\right) \tag{12}$$

is maximized subject to the moment constraint Eqs. (9), (10) and (11). The $\hat{p}_n$ in Eq. (12) represent a default model chosen empirically. Details of default models as well as the practical aspects relating to calculation of moments and the maximization procedure are given elsewhere (see [24]). A flat default model ($\hat{p}_n = 1$ for $n \le n_{max}$ and $\hat{p}_n = 0$ otherwise) results in a discrete Gaussian-like form of p_n with given mean and variance. Maximization using the Lagrange multiplier method gives [17]

$$p_n = \hat{p}_n e^{\lambda_0 + \lambda_1 n + \lambda_2 n^2}, \tag{13}$$

where λ_0, λ_1, and λ_2 are Lagrange multipliers that are chosen to satisfy the constraint Eqs. (9)–(11). For a flat default model, the above equation can be written in an approximate but more familiar form as,

$$p_n \approx \frac{1}{\sqrt{2\pi \langle \delta n^2 \rangle}} \exp\left[-\frac{(n - \rho v)^2}{2 \langle \delta n^2 \rangle} \right], \tag{14}$$

where $\langle \delta n^2 \rangle = \langle (n - \langle n \rangle)^2 \rangle$ is the variance of the number of particles in a given molecular volume v.

2.3. Attractive contributions to the chemical potential

Formally, the attractive contribution in Eq. (6) is given by,

$$\langle u_{att}\rangle_{WCA} = \int_0^\infty 4\pi r^2 \rho u_{att}(r) g_{WCA-O}(r) dr, \quad (15)$$

where $g_{WCA-O}(r)$ is the radial distribution function between the *WCA* reference solute and water oxygen. The exact functional form of $g_{WCA-O}(r)$ is determined by the potential of mean force (PMF) between a water molecule and the reference solute. It was found previously that, for reasonably small solutes, the solvent-mediated contribution to the solute–water PMF is practically independent of solute–water interactions (i.e. independent of solute–water σ and ϵ), after its appropriate radial translation to account for solute size differences [16]. Thus, for weak solute–water interactions, the water structure around the solute is approximately identical for various solutes, except for its trivial radial translation [16,26,27]. The subtle effects of a 'cavity expulsion potential' [16] come into play in any significant manner only for much larger solutes ($\sigma > 0.5$ nm). The $g_{WCA-O}(r)$ can thus be approximated by a single functional form for a variety of solutes.

Use of an accurate form of the 'universal' solvent-mediated solute–water potential of mean force in a perturbation approach to calculate $g_{WCA-O}(r)$ constitutes a truly molecular theory for the solute–water attractive interactions [16]. Qualitatively, the attractive contribution is expected to be dominated by the long range part of the solute–water interactions where details of $g_{WCA-O}(r)$ are less important. Hence, we make a crude approximation for $g_{WCA-O}(r)$ as follows:

$$g_{WCA-O}(r) \approx \begin{cases} 0 & \text{for } r < \sigma \\ g_{\max} & \text{for } \sigma \le r \le 2^{1/6}\sigma \\ 1 & \text{for } r > 2^{1/6}\sigma \end{cases} \quad (16)$$

$g_{\max}$ can be interpreted as the height of the first peak of the *WCA* solute–water radial distribution function. The position of the first peak of $g_{WCA\text{-}O}(r)$ is expected to be between σ and $2^{1/6}\sigma$ (see [16]). Thus, the $g_{\max}$ part of the radial distribution function represents approximately the contribution from the attractive interactions with water in the first hydration shell. In that sense, $g_{\max}$ can be considered as an adjustable parameter. Such a crude representation is deliberate for it allows us to understand how the attractive contribution depends on the properties of pure water and solute–water attractive interactions. Also, simple relationships become apparent that are hidden in an exact treatment. Integrating Eq. (15) using this simple model for the radial distribution function, we obtain

$$\langle u_{att}\rangle_{WCA} \approx -\frac{4\pi\rho\epsilon\sigma^3}{3}\left[g_{\max}(\sqrt{2}-1) + 5\sqrt{2}/3\right] \quad (17)$$

This expression constitutes the second part of the solute chemical potential in terms of quantities that are readily available. In particular, the attractive contribution is directly proportional to the bulk water density ρ, the solute–water attractive interaction parameter ϵ, and the volume of the solute $4\pi\sigma^3/3$. In what follows we use Monte Carlo simulations to verify the validity of the approximations leading to Eqs. (6) and (17).

2.4. Computer simulations and test particle insertions

Monte Carlo (MC) simulations of 256 simple point charge (SPC) water [28] molecules were performed in the canonical ensemble [29]. Simulations were carried out at eight different temperatures between 280 K and 470 K along the experimental saturation curve of water [10]. Ewald summation was used for electrostatic interactions [30,31]. 150 000 Monte Carlo passes were used for equilibration followed by 250 000 passes for production, where one pass corresponds to an attempted MC move of each water molecule. Water configurations were saved during the production run every 25 passes. Thus, a total of 10 000 configurations were used for further analysis. Approximately 36 h of CPU time were required for 400 000 passes performed at each temperature on an SGI R10K processor.

Water oxygen–oxygen radial distribution functions were calculated from the pure water configurations and were used as input to the information theory calculations [24]. Water configurations were also used to perform exhaustive test particle insertion calculations. Nine different solutes were chosen for the these insertions. *LJ* parameters for these solutes are given in Table 1. The solutes M1, Me, M2, and M3 have the same σ, whereas, the *LJ* well depth ϵ is varied from $\epsilon_{Me-Me}/2$ for the solute M1 to $4\epsilon_{Me-Me}$ for the solute M3. For the solutes M4 and M5, the well depth is ϵ_{Me-Me}, and the solute–solute σ is chosen to give the solute–water σ of 0.32 and 0.36 nm, respectively. Lorentz–Berthelot rules were used to calculate the solute–water interaction energy parameters [29]. Solutes M4, Me, and M5, thus, have the same *LJ* well depth and increasing sizes. For each solute, the corresponding *WCA* and *HS* equivalents were also considered in the test particle simulations, amounting to a total of 27 solutes.

Eight million insertions per configuration for each solute were performed on a cubic grid with mesh size of approximately 0.01 nm. The box volume was sampled initially with a test solute with the corresponding cavity radius equal to 0.28 nm. Insertions of solutes were then performed only at positions where the insertions of the test solute were successful. The cavity radius of the test solute of 0.28 nm is at least 0.02 nm smaller than the equivalent cavity radii of all the solutes considered here. Using a test radius of 0.24 nm did not change the results reported here. Appropriate normalizations were performed to calculate averages. A total of approximately 4 h of CPU time was required at each temperature on an SGI R10K processor.

The excess chemical potentials of *LJ*, *WCA*, and *HS* solutes, the corresponding attractive contributions $\langle u_{att}\rangle_{WCA}$, and solute–water interaction energies $\langle u_{SW}\rangle$, were calculated for each solute using [13],

$$\mu^{ex} = -k_B T \ln\left\langle \exp\left(-\frac{u_{SW}}{k_B T}\right)\right\rangle_W \tag{18}$$

Table 1
LJ parameters for solute-solute and water-water interactions [13,29]

Solute	σ/nm	ϵ/(kJ/mol)
Ar	0.3415	1.0393
Kr	0.3675	1.4052
Xe	0.3975	1.7852
M1	0.3730	0.6132
Me	0.3730	1.2264
M2	0.3730	2.4528
M3	0.3730	4.9056
M4	0.3234	1.2264
M5	0.4034	1.2264
H_2O	0.3166	0.6502

$$\langle A\rangle = \frac{\left\langle A\exp\left(-\frac{u_{SW}}{k_B T}\right)\right\rangle_W}{\left\langle \exp\left(-\frac{u_{SW}}{k_B T}\right)\right\rangle_W}, \tag{19}$$

where $\langle A\rangle$ represents the average of the quantity A (e.g. u_{SW}) in the solute–water system. The averages on the right hand side are calculated for the pure water system. Solute–water radial distribution functions were also calculated by averaging appropriate delta functions. For the *HS* solutes, only chemical potentials and *HS*–water radial distribution functions were calculated.

3. Results and discussion

3.1. Chemical potentials

Fig. 1 shows excess chemical potentials in units of $k_B T$ for the solutes M1, Me, M2, and M3 with *LJ*, *WCA*, and *HS* solute–water interactions. For the structural definition of the *HS* radius used here, we find that the excess chemical potentials of *WCA* solutes are approximately one $k_B T$ higher than those of *HS* solutes. Note, however, that the temperature dependences of both *WCA* and its equivalent *HS* solutes are approximately identical. Beyond $\sim$280 K, $\mu/k_B T$ for both the solutes decrease monotonically with temperature.

The contribution from solute–water attractive interactions $\langle u_{att}\rangle_{WCA}$ is also shown in Fig. 1 in k_{BT} units. The magnitude of the attractive energy decreases with increasing temperature. Further-

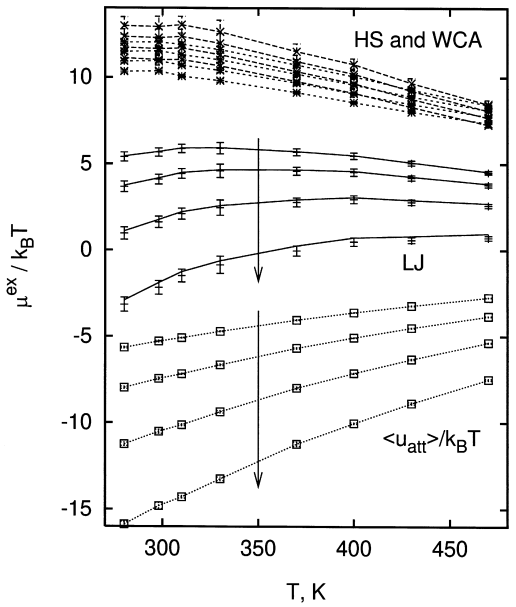

Fig. 1. Excess chemical potentials of *LJ* (+), *WCA* (×), and *HS* solutes (*) in k_BT units calculated using test particle insertions. The arrows indicate curves corresponding to the order of solutes: M1, Me, M2, and M3. The attractive contribution $\langle u_{att}\rangle_{WCA}/k_BT$ is also shown (□). Chemical potentials of *LJ* solutes calculated using Eq. (6) (solid lines) are compared with actual insertion results (symbols with error bars; one standard deviation calculated using block averages).

more, Fig. 1 shows the excess chemical potentials of the *LJ* solutes calculated from simulations as well as by adding the $\langle u_{att}\rangle_{WCA}$ term to the chemical potentials of corresponding *WCA* solutes. These are indistinguishable from the excess chemical potentials of *LJ* solutes calculated from simulations, which shows that the approximations leading to Eq. (6) are reasonable for the solutes studied here. Note that the temperature dependence of μ^{ex}_{LJ}/k_BT is non-monotonic. This behavior leads to a solubility minimum for these solutes in water, which we discuss in the following section.

3.2. Information theory model

Having verified the validity of the approximations made in Section 2.1 we next compare the predictions of excess chemical potentials for *HS* solutes using information theory with those calculated from test particle insertions. Bulk water densities and water oxygen–oxygen radial distribution functions were used to calculate the first and second moment of the particle number distributions. The excess chemical potentials of the *HS* solutes M1, Me, M2, M3, and Xe, calculated from information theory using a flat default model are shown in Fig. 2. Also shown are the corresponding excess chemical potentials calculated from test particle insertions. The agreement between the two is excellent except at intermediate temperatures where slight underpredictions of excess chemical potentials are observed. Overall, both the absolute value as well as the temperature dependence of the chemical potentials are predicted well using the information theory approach.

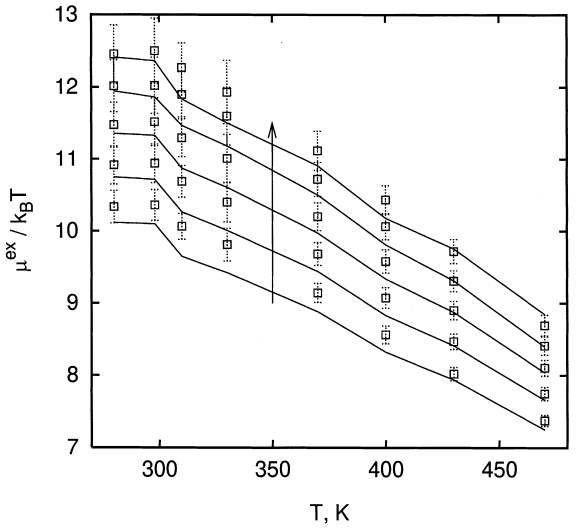

Fig. 2. Excess chemical potentials of *HS* solutes calculated using test particle insertions (symbols). The lines are information theory predictions made using bulk water density and the water oxygen–oxygen radial distribution function. The arrow indicates curves corresponding to the order of solutes: M1, Me, M2, M3, and Xe.

3.3. Attractive interactions

In Eq. (17), the attractive contributions to the solute excess chemical potential are related to the

bulk water density ρ and parameters of the solute–water interactions: the *LJ* well depth ϵ, and the solute size σ. To verify the accuracy of Eq. (17), we define the ratio C of the attractive contribution calculated from test particle insertions and that given by Eq. (17),

$$C = \frac{\langle u_{att} \rangle_{simulation}}{\langle u_{att} \rangle_{eq.17}}. \tag{20}$$

For an accurate description of $g_{WCA-O}(r)$ in Eq. (16), the ratio C will be equal to one, independent of solute–water interaction parameters as well as temperature. Fig. 3 shows the C calculated using $\langle u_{att} \rangle_{WCA}$ obtained from test particle insertions for the nine *LJ* solutes listed in Table 1. $g_{\max}$ in Eq. (17) is assumed to be equal to 2.0, approximately the height of the first peak of the methane–water oxygen radial distribution function. Also, $g_{\max}$ is assumed to be constant, independent of temperature as well as the type of solute. Remarkably, we find C to be close to one ($1.15 > C > 1$) and independent of the type of solute, even when using a surprisingly simple description of the reference solute–water radial distribution function. Only a weak temperature dependence of C is observed that is due to the assumption of constancy of $g_{\max}$ with respect to temperature. This relative insensitivity of $\langle u_{att} \rangle_{WCA}$ to the details of $g_{WCA-O}(r)$ is expected from Eq. (17). The two terms in the brackets, representing short-range and long-range contributions to $\langle u_{att} \rangle_{WCA}$, are $0.414 g_{\max}$ and $5\sqrt{2}/3$, equal to 0.83 and 2.36, respectively, for $g_{\max} = 2$. In other words, a 25% change in $g_{\max}$ leads to only approximately 6% change in the final value of $\langle u_{att} \rangle_{WCA}$.

Thus, we have shown that both the repulsive as well as attractive contributions to the solute excess chemical potentials can be modeled quantitatively using readily available information, such as the bulk density and radial distribution function of water, and an empirically obtained constant $C \approx 1$. In the following section, we use these simple models to understand the molecular origin of the solubility minimum of non-polar gases in water.

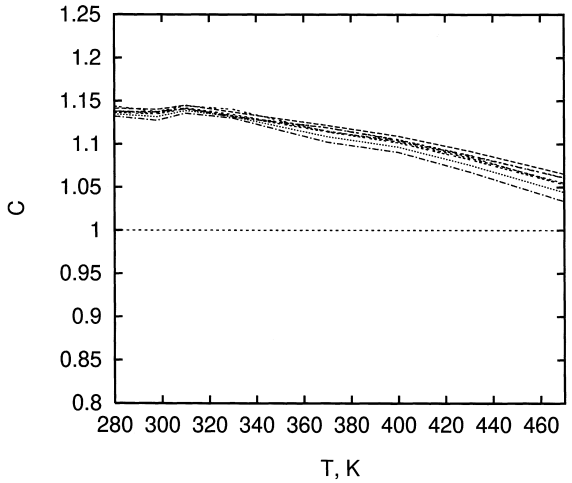

Fig. 3. The ratio C in Eq. (20) calculated using test particle insertion data. Values of C for all the nine different solutes are shown. $g_{\max}$ is assumed to be 2.00 for all solutes at all temperatures. The dashed line, $C = 1$, is shown for reference.

3.4. Origin of the solubility minimum

Ostwald's partition coefficient L of a solute between a gas phase and water is defined as [19,11]

$$L = \frac{\rho_S^W}{\rho_S^g} = \exp\left[-\frac{(\mu_W^{ex} - \mu_g^{ex})}{k_B T} \right], \tag{21}$$

where ρ_S^g and ρ_S^W are the number densities of the solute in the gas and the water phase in thermodynamic equilibrium, respectively, and μ_g^{ex} and μ_W^{ex} are solute excess chemical potentials in the gas and the water phase, respectively. Since we are interested in the solubility behavior below ~ 400 K, we can assume that the gas phase is ideal [11,13], that is, $\mu_g^{ex} = 0$. In that case, $L = \exp(-\mu^{ex}/k_B T)$, where the subscript W has been omitted for notational simplicity. Thus, a minimum in L with temperature arises from the maximum in $\mu^{ex}/k_B T$. As shown in Fig. 4, $\mu^{ex}/k_B T$ curves for *LJ* solutes calculated from test particle insertions indeed show a maximum for the different *LJ* solutes studied here. The temperature corresponding to the solubility minimum increases with increasing strength of solute–water attractive interactions. In contrast, $\mu^{ex}/k_B T$ for

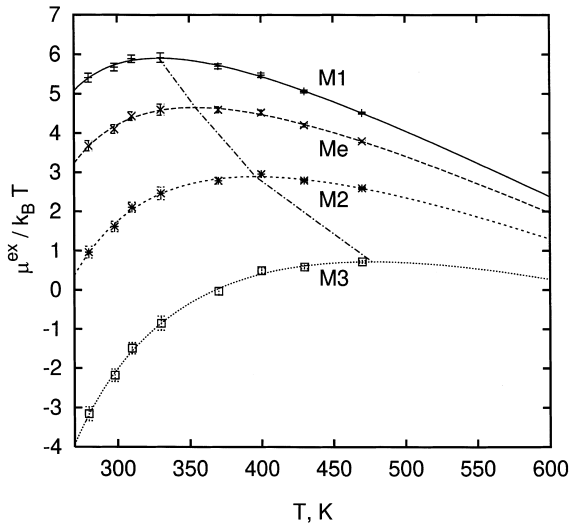

Fig. 4. $-\ln L = \mu^{ex}/k_B T$ as a function of temperature calculated for *LJ* solutes using test particle insertions. The lines are rational function fits to the data and are used to locate accurately the temperature of solubility minimum. The dash–dot line shows the position of the maximum of $\mu^{ex}/k_B T$ for each curve.

both *WCA* and *HS* solutes decrease monotonically with temperature in this range (see Figs. 1 and 2). The maximum value of $\mu^{ex}/k_B T$ for all *WCA* and *HS* solutes is found at approximately 280 K. The attractive contributions change this behavior. As shown in Fig. 1, the $\langle u_{att}\rangle_{WCA}/k_B T$ term is more negative at lower temperatures and decreases in magnitude at higher temperatures. Addition of the attractive contributions, thus, lowers the chemical potentials near room temperature more than it does at higher temperatures. As a result, the maximum in $\mu^{ex}/k_B T$ obtained for strictly repulsive solutes shifts from $T \approx 280K$ to higher temperatures, depending on the strength of attractive interactions.

This behavior can be understood using the simple models developed here for the repulsive and attractive interactions. For a hard sphere solute, we use a continuous Gaussian approximation for the water occupancy-number fluctuations [10],

$$\frac{\mu^{ex}_{HS}}{k_B T} \approx \frac{\rho^2(T) v^2}{2\langle \delta n^2\rangle} + \tfrac{1}{2}\ln(2\pi\langle \delta n^2\rangle), \qquad (22)$$

where v is the volume of the *HS* solute. Since the second term will be smaller than the first and only logarithmically sensitive to the variance $\langle \delta n^2\rangle$, we can reasonably neglect it for this approximate analysis. Furthermore, we find that $\langle \delta n^2\rangle$ has a negligible dependence on temperature in the range of temperatures considered here [10][2]. In the macroscopic limit, the particle number variance $\langle \delta n^2\rangle$ is related to the isothermal compressibility of water which is also relatively insensitive to the temperature compared to, for example, organic liquids [24,32]. Thus, the temperature dependence of $\mu^{ex}/k_B T$ arises almost entirely from the $\rho^2(T)$ term. $\mu^{ex}/k_B T$ then reaches a maximum for both the *HS* and *WCA* solutes at a temperature corresponding approximately to the maximum in density of pure water (277 K)!

A similar analysis can be used to understand the temperature dependence of $\mu^{ex}/k_B T$ for *LJ* solutes. For *LJ* solutes,

$$\frac{\mu^{ex}_{LJ}}{k_B T} \approx \frac{\rho^2(T) v^2}{2\langle \delta n^2\rangle} + \tfrac{1}{2}\ln(2\pi\langle \delta n^2\rangle) - C\left[g_{\max}(\sqrt{2}-1) + 5\sqrt{2}/3\right]\frac{4\pi\sigma^3\epsilon\rho(T)}{3k_B T}$$

$$\approx C_1\,\rho^2(T)\sigma^6 - C_2\frac{\sigma^3\epsilon\rho(T)}{T} \qquad (23)$$

where $C_1 = 8\pi^2/9\langle \delta n^2\rangle$, $C_2 = 4\pi C[g_{\max}(\sqrt{2}-1) + 2\sqrt{2}]/3k_B$, $v = 4\pi\sigma^3/3$, and we have neglected the logarithmic term, as described above. Fig. 5 illustrates the repulsive and attractive contributions to the *LJ* solute excess chemical potential in units of $k_B T$ for solutes with different interaction parameters. The solid curve shows $\mu^{ex}/k_B T$ for the *HS* solute with $\sigma = 0.35$, the first term in Eq. (23). $\langle \delta n^2\rangle$ for this solute is approximately 1.3. Also shown are $\mu^{ex}/k_B T$ for *LJ* solutes calculated by adding the second term

[2]The variance $\langle \delta n^2\rangle$ has two contributions: ρv and $\rho^2 \int_v \mathrm{d}\mathbf{r} \int_v d\mathbf{r}'[g(\mathbf{r},\mathbf{r}')-1]$, where $g(\mathbf{r},\mathbf{r}')$, is the water–water radial distribution function. The former is positive and decreases with temperature, whereas the latter is negative and increases with temperature. The total, however, is remarkably insensitive to temperature.

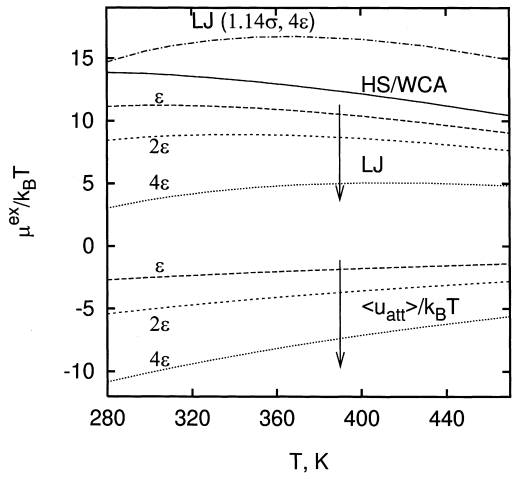

Fig. 5. The excess chemical potentials of model *LJ* solutes in k_BT units calculated using Eq. (23) for $\sigma = 0.35$ nm, $\epsilon = 0.3$ kJ/mol. The chemical potential curve for the corresponding HS solute calculated using Eq. (22) is also shown (the logarithmic term is neglected). The three curves for *LJ* solutes correspond to attractive interactions of ϵ, 2ϵ, and 4ϵ, respectively. The top curve shows the variation of the chemical potential for a solute with parameters, $\sigma = 0.40$ nm, and $\epsilon = 1.2$ kJ/mol.

in Eq. (23), that is the $\langle u_{att} \rangle_{WCA}$ term, for three different *LJ* well depths, ϵ, 2ϵ, and 4ϵ, respectively. Increasing the strength of attractive interactions makes the chemical potential favorable as well as shifts the temperature corresponding to the maximum of μ^{ex}/k_BT to higher values. Thus, in general, the more attractive the solute–water interactions, the higher the temperature corresponding to the solubility minimum. In contrast, for solutes with weak attractive interactions with water, the solubility minimum will be close to that for *HS* or *WCA* solutes, equal to ~ 277 K, and at room temperature, the solubility of these solutes will increase monotonically with temperature.

In this simple model, the solute size has an effect on the temperature of solubility minimum opposite to that of ϵ. For larger solutes, the *HS* contribution is higher. Correspondingly, the value of the chemical potential increases and the temperature of solubility minimum shifts to a lower value, as illustrated in the top curve in Fig. 5 for a solute with $\sigma = 0.40$ nm and $\epsilon = 1.20$ kJ/mol.

4. Conclusions

The theoretical development presented in this paper has led to a simple molecular model for the temperature dependence of chemical potentials of *LJ* solutes in water. The hydration of a *LJ* solute is divided into two steps. The reversible work required for the formation of a cavity of the shape and size of the solute is calculated using an information theory approach [17]. We find that using only readily available properties of bulk water — water number density and water oxygen–oxygen radial distribution function — information theory provides quantitative estimates of chemical potentials of *HS* solutes — the repulsive part of the *LJ* solute chemical potential. Using ideas regarding water structure in the vicinity of non-polar solutes developed recently [16], we find that a surprisingly simple representation of the solute–water radial distribution functions leads to a quantitative description of the attractive interactions between solutes and water.

The expression for the excess chemical potentials of *LJ* solutes obtained here is remarkably simple. We find that the variance of particle number fluctuations in molecular-scale volumes is almost independent of temperature up to a temperature of ~ 450 K [10]. The macroscopic expression of this behavior is the *relative* temperature insensitivity of the water isothermal compressibility compared to hydrocarbon liquids; in comparison to benzene, normal alkanes, and carbon tetrachloride, the isothermal compressibility of liquid water varies only weakly along the saturation curve up to 450 K [32]. The temperature dependence of both repulsive as well as attractive contributions, thus, arises predominately from the temperature dependence of the bulk water density. This information is contained in the equation of state of pure water. For given solute–water interaction parameters, Eq. (23) then represents the sort of simple relationship of solute chemical potentials with macroscopic observable properties of water that we set out to derive in the beginning.

The thermodynamic properties of hydration can

be calculated by modeling the excess chemical potentials. Near room temperature, the entropy of hydration is large and negative, whereas the heat capacity of hydration is large and positive [10,33]. At the extremum of μ^{ex}/k_BT, its temperature derivative, $-H^{ex}/k_BT^2$ is zero, where H^{ex} is the excess enthalpy of hydration. Furthermore, the second derivative at the extremum, $-C_p^{ex}/k_BT^2$, where C_p^{ex} is the excess heat capacity of hydration at constant pressure, is negative, consistent with a maximum of μ^{ex}/k_BT. A more detailed investigation into the thermodynamic properties of hydration in the first — cavity formation — and the second — attractive interactions — step will shed light on the solvent reorganization contributions [27].

The solute size and strength of attractive interactions can be related, in principle, to critical properties, such as the critical temperature, pressure, and volume. Such a connection is clear for pure solute phases obeying a van der Waals equation of state [34]. Qualitatively, gaseous solutes with higher critical temperatures, for example, close to ambient temperature, will have more favorable attractive interactions compared to those with critical temperatures lower than the ambient temperature. Following the discussion in the preceding section, more favorable attractive interactions imply a higher temperature for the solubility minimum [35]. Such a correlation is indeed observed in experimental data on the solubility of a variety of gases in water [35].

An interesting connection can be made between these results and recent experimental data on the effects of temperature and surfactant chain length on the CMC of surfactants [9]. It is well-known that, as a function of temperature, the CMCs of both non-ionic and ionic surfactants exhibit a minimum near room temperature. The minimum in the solubility of the hydrophobic tails in water would lead to the minimum in CMC of a surfactant. The dependence of $T_{\min}$, the temperature of CMC minimum, on the surfactant length is also interesting. Here we consider non-ionic C_iE_j surfactants, where i and j are the numbers of methylene groups C and ethylene oxide groups E, the hydrophobic and the hydrophilic parts, respectively. Recent experimental data [9] show that the effect of chain lengths of hydrophobic (i) and hydrophilic (j) parts on $T_{\min}$ are similar to those of solute size (σ) and the strength of the solute–water attractive interaction (ϵ), respectively, on the temperature for solubility minimum. For surfactants $C_{12}E_4$, $C_{12}E_6$, and $C_{12}E_8$, the values of $T_{\min}$ are 46, 49, and 52°, respectively [9]. Thus, increasing the length of the hydrophilic part, that is, the attractive interactions, increases $T_{\min}$. On the other hand, the values of $T_{\min}$ for surfactants $C_{10}E_8$, $C_{12}E_8$, and $C_{14}E_8$ are 61, 52, and 46°, respectively [9]. This trend is again expected from the modeling presented here. A quantitative prediction of $T_{\min}$, however, will require detailed modeling of the thermodynamics of micelle formation.

Finally, we note that the phenomenon of a minimum in the solubility of gases in liquids is not special to water, but is observed for common gases in organic liquids [11,12] as well as in polymers [36]. The modeling presented here can be readily extended to those liquids as well [37].

Acknowledgements

S.G. acknowledges Dr. Hank Ashbaugh and Prof. Michael E. Paulaitis for numerous insightful discussions as well as a critical reading of the manuscript. S.G. is a Director's Funded Postdoctoral Fellow at the Los Alamos National Laboratory. This work was supported by the US Department of Energy through Los Alamos National Laboratory-Directed Research and Competency Development grant for an 'Integrated Structural Biology Resource'.

References

[1] W. Kauzmann, Adv. Protein Chem. 14 (1959) 1.
[2] C. Tanford, The Hydrophobic Effect: Formation of Micelles and Biological Membranes, John Wiley, New York, 1973.
[3] K.A. Dill, Biochemistry 29 (1990) 7133.
[4] W. Blokzijl, J.B.F.N. Engberts, Angew. Chem. Int. Ed. Engl. 32 (1993) 1545.
[5] P.L. Privalov, Adv. Protein Chem. 33 (1979) 167.
[6] R.L. Baldwin, Proc. Natl. Acad. Sci. USA 83 (1986) 8069.
[7] W. Kauzmann, Nature 325 (1987) 763.

[8] G. Hummer, S. Garde, A.E. García, M.E. Paulaitis, L.R. Pratt, Proc. Natl. Acad. Sci. USA 95 (1998) 1552.
[9] L.-J. Chen, S.-Y. Lin, C.-C. Huang, J. Phys. Chem. B 102 (1998) 4350.
[10] S. Garde, G. Hummer, A.E. García, M.E. Paulaitis, L.R. Pratt, Phys. Rev. Lett. 77 (1996) 4966.
[11] G.L. Pollack, Science 251 (1991) 1323.
[12] J.M. Prausnitz, Molecular Thermodynamics of Fluid-Phase Equilibria, Prentice-Hall, Englewood Cliffs, New Jersey, 1986.
[13] B. Guillot, Y. Guissani, J. Chem. Phys. 99 (1993) 8075.
[14] G. Graziano, J. Chem. Soc. Faraday Trans. 94 (1998) 3345.
[15] L.R. Pratt, D. Chandler, J. Chem. Phys. 67 (1977) 3683.
[16] G. Hummer, S. Garde, Phys. Rev. Lett. 80 (1998) 4193.
[17] G. Hummer, S. Garde, A.E. García, A. Pohorille, L.R. Pratt, Proc. Natl. Acad. Sci. USA 93 (1996) 8951.
[18] J.D. Weeks, D. Chandler, H.C. Andersen, J. Chem. Phys. 54 (1971) 5237.
[19] A. Ben-Naim, Hydrophobic Interactions Plenum Press, New York, 1980.
[20] R.W. Zwanzig, J. Chem. Phys. 22 (1954) 1420.
[21] B. Widom, J. Phys. Chem. 86 (1982) 869.
[22] J.-P. Hansen, I.R. McDonald, Theory of Simple Liquids Academic Press, New York, 1986.
[23] H. Reiss, H.L. Frisch, J.L. Lebowitz, J. Chem. Phys. 31 (1959) 369.
[24] G. Hummer, S. Garde, A.E. García, M.E. Paulaitis, L.R. Pratt, J. Phys. Chem. 102 (1998) 10469.
[25] J.E. Shore, R.W. Johnson, IEEE Trans. Inf. Theory, IT 26 (1980) 26.
[26] S. Garde, G. Hummer, A.E. García, L.R. Pratt, M.E. Paulaitis, Phys. Rev. E 53 (1996) R4310.
[27] H.S. Ashbaugh, M.E. Paulaitis, J. Phys. Chem. 100 (1996) 1900.
[28] H.J.C. Berendsen, J.P.M. Postma, W.F. van Gunsteren, J. Hermans, in: B. Pullman (Ed.), Intermolecular Forces: Proceedings of the 14th Jerusalem Symposium on Quantum Chemistry and Biochemistry, Reidel, Dordrecht, Holland, 1981, pp 331–342.
[29] M.P. Allen, D.J. Tildesley, Computer simulation of liquids, Clarendon Press, Oxford, UK, 1987.
[30] P.P. Ewald, Ann. Phys. 64 (1921) 253.
[31] G. Hummer, L.R. Pratt, A.E. García, J. Phys. Chem. 99 (1995) 14188.
[32] J.S. Rowlinson, F.L. Swinton, Liquids and Liquid Mixtures, Butterworth Scientific, London, 1982.
[33] T.R. Rettich, Y.P. Handa, R. Battino, E. Wilhelm, J. Phys. Chem. 85 (1981) 3230.
[34] D.A. McQuarrie, Statistical Mechanics, Harper-Collins, New York, 1976.
[35] S.I. Sandler, Chemical and Engineering Thermodynamics, John-Wiley, p. 438, New York, 1989.
[36] J.G. Curro, K.G. Honnell, J.D. McCoy, Macromolecules 30 (1997) 145.
[37] S. Garde, R. Khare, G. Hummer, unpublished, 1998.